Proceedings of the 5th International Conference on Inverse Problems in Engineering: Theory and Practice, Cambridge, UK, 11-15th, July 2005

FINITE ELEMENT APPROACH TO INVERSE PROBLEMS IN DYNAMIC ELASTOGRAPHY

A. M. MANIATTY and E. PARK
Department of Mechanical, Aerospace and Nuclear Engineering, Rensselaer Polytechnic Institute, Troy, New York 12180, USA
e-mail: maniaa@rpi.edu and parke@rpi.edu
Tel: 518-276-6984, Fax: 518-276-6025

Abstract - Conventional ultrasound and MRI can be used to measure tissue displacement while it is subjected to pulses that induce motion. This paper presents preliminary work towards analyzing such displacement data to reconstruct quickly and robustly the shear modulus field to be used as a potential medical diagnostic tool. For now, we treat the tissue as an isotropic, elastic, relatively incompressible media. We consider the complete equations for linear, isotropic, elasto-dynamics. A finite element model of this system is used as a basis. Two solution approaches are discussed: a direct inversion approach and an iterative approach. The advantages of the direct inversion approach are the speed, since iterations are not needed, and that it does not over-weight boundary data. The advantage of the iterative approach is that it does not require differentiation of data. Results using the direct inversion approach are presented and discussed.

1. INTRODUCTION

The elastic properties of soft tissue are directly related to the underlying structure of the tissue and are therefore strongly affected by pathological changes in the tissue. Indeed, palpation is a very old and standard medical practice for detecting irregularities in the elastic stiffness of tissue. However, palpation is limited to detecting stiffness changes that are sufficiently large and near the surface. Elastography [14] is a promising new diagnostic technology based on imaging mechanical attributes of tissue to detect smaller and deeper irregularities than can be detected by palpation.

To be specific, it is the elastic resistance to shape change that is most affected by pathological changes. For isotropic materials, this is characterized by the shear modulus. For example, the shear modulus in breast cancer is typically 7 to 28 times stiffer than normal tissue [16, 19, 11] and about 8 times stiffer than benign fibroadenomas [19]. Thus, imaging the shear modulus has the potential of providing high contrast images that differentiate between various pathological states of the tissue. On the other hand, the bulk modulus, or resistance to volume change, is relatively very large (typically six orders of magnitude higher than the shear modulus) and varies little in soft tissue.

Elastography involves inducing a static compression [14, 10, 15], harmonic vibration [20, 9], or a transient pulse [4, 18] in the tissue and recording the mechanical response, typically the displacement field. Either ultrasound or MRI is used to measure the tissue displacement. The use of a time harmonic excitation is more common than a transient excitation because conventional ultrasound and MRI systems do not have a sufficiently high frame rate to capture a transient wave in a single experiment. Elastographic images generated can be classified as either images of quantities directly obtained from the tissue displacement measurements and its derivatives (strain [15], displacement amplitude and vibration phase [8]) or as images of the elastic stiffness [1, 7] indirectly determined from the displacement measurements using the governing equations relating the tissue motion and the elastic properties. While the first type of images are easier to generate because they come directly from the measured displacement data, the second type are more informative as they show the properties of the tissue which are affected by the underlying structure and pathological changes in the tissue. The problem of reconstructing the elastic stiffness from the displacement measurements is an inverse problem of parameter identification.

This work focuses on solving this inverse problem for time harmonic induced tissue excitations. In most of the elastography literature, when the elastic shear modulus (or Young's modulus or shear wave speed, which are directly related to the shear modulus) is reconstructed, two assumptions are used to reduce the equations of motion down to the Helmholtz equation where the displacement components decouple, see for example [2, 12]. These assumptions are that the gradient of the hydrostatic stress (or pressure) is negligible, and the shear modulus can be treated as locally constant. In this work, these assumptions are not made, and the complete governing equations for linear, isotropic, elasto-dynamics are considered. A weak form of the governing equations is used to reduce the derivatives required on the

data, and finite element interpolations are used to convert the problem into a finite dimensional subspace. Two approaches are discussed, an iterative approach, similar to that presented in van Houten *et al.* [6, 7], and a direct approach. Results from the direct approach are presented.

Finally, it should be mentioned that, in general, the mechanical behavior of soft tissue is much more complex than the simple linear, isotropic, elastic assumption made here. In general, it is anisotropic, viscoelastic, and non-linear, see for example Fung [5]. In this work, only very small amplitude excitations about a reference strain are considered, making geometric linearity a valid approximation. For dynamic excitations, viscous effects alter the wave speed and lead to attenuation. These effects are stronger at higher frequencies. For this reason, experimentalists have focused on using low frequency excitations, typically tens or hundreds of Hz. At these frequencies, for typical tissue viscoelastic properties, the wavespeed is altered less than 1% from what it would be for a purely elastic material (i.e. if the viscosity was set to zero), but the attenuation may be more significant (up to a few percent per cm). For elastography, this results in a lower signal to noise ratio as the wave travels through the tissue. However, the isotropic assumption is likely the bigger source of error. While some tissue is fairly isotropic, such as fatty tissue, most tissue exhibits some anisotropy, for example fibrous tissue or tissue with blood vessels or ducts running through it. Although anisotropy and viscoelastic effects are not considered here, they are starting to be investigated by these authors and others [4, 17]. This work presents a first step with a simple model that captures the first order effects and is reasonable in certain circumstances.

2. GOVERNING EQUATIONS AND PROBLEM DEFINITION

2.1 Forward Problem

The usual forward problem in linear, elasto-dynamics consists of finding the displacement field, $\boldsymbol{u}(\boldsymbol{x},t)$ which depends on position $\boldsymbol{x}\in\Omega$ and time $t\in\tau$ satisfying

$$\begin{aligned}
\left[\mu\left(u_{i,j}+u_{j,i}\right)\right]_{,j}+p_{,i} &= \rho\ddot{u}_i \quad \text{in } \Omega\times\tau \quad \left({}_{,j}\equiv\frac{\partial}{\partial x_j}\right) && (1)\\
p &= \lambda u_{k,k} && (2)\\
u_i &= \hat{u}_i \quad \text{on } \partial\Omega_{1i}\times\tau && (3)\\
\left[\mu\left(u_{i,j}+u_{j,i}\right)+p\delta_{ij}\right]n_j &= \hat{T}_i \quad \text{on } \partial\Omega_{2i}\times\tau && (4)\\
u_i(\boldsymbol{x},0) &= u_i^0 \quad \text{in } \Omega && (5)\\
\dot{u}_i(\boldsymbol{x},0) &= \dot{u}_i^0 \quad \text{in } \Omega && (6)
\end{aligned}$$

where $\mu(\boldsymbol{x})$ is the shear modulus, which depends on position, $p(\boldsymbol{x},t)$ is a hydrostatic stress, which depends on position and time, ρ is the density, and λ is a Lamé parameter. Equations (1) and (2) together are the balance of linear momentum. It should be noted that for soft tissue, the Lamé parameter, $\lambda(\boldsymbol{x})\gg\mu(\boldsymbol{x})$, is about six orders of magnitude higher than μ (typical value for λ is 2.3 GPa, while μ is of the order of kPa). For stability purposes, a mixed formulation, as given in equations (1) and (2), where the hydrostatic stress, p, is introduced as an additional variable, is typically used [3]. Equations (3) and (4) are boundary conditions on the displacements and tractions, and Equations (5) and (6) are initial conditions on the displacement and velocity fields. Finally, for completeness, either type of boundary condition must be specified at each location on the boundary in each direction for all time without overlap, $\partial\Omega_{1i}\cup\partial\Omega_{2i}=\partial\Omega$ and $\partial\Omega_{1i}\cap\partial\Omega_{2i}=\emptyset$.

As mentioned in the introduction, one of the most common excitations used in elastography is a time harmonic excitation, and the displacement is field is measured at several times. Thus, to simulate a typical experiment, a time harmonic displacement field is assumed taking on the form

$$u_i(\boldsymbol{x},t)=\check{u}_i(\boldsymbol{x})\sin(\omega t) \tag{7}$$

where ω is the angular frequency of excitation and $\check{\boldsymbol{u}}(\boldsymbol{x})$ is the amplitude of the displacement field. Substituting into equations (1) and (2) yields

$$\begin{aligned}
\left[\mu\left(\check{u}_{i,j}+\check{u}_{j,i}\right)\right]_{,j}+\check{p}_{,i} &= -\rho\omega^2\check{u}_i && (8)\\
\check{p} &= \lambda\check{u}_{k,k} && (9)
\end{aligned}$$

which depends only on spatial position. These equations, together with boundary conditions (3) and (4) yield a boundary value problem for the time harmonic case. Forward solutions with this formulation yield displacement fields very similar to those observed in experiments.

2.2 Inverse Problem

The inverse problem of interest here, involves finding the shear modulus, $\mu(\boldsymbol{x})$ that best satisfies equations (8) and(9) given some measurements of the displacement field amplitude at discrete locations,

$$\breve{u}_i(\boldsymbol{x}_p) \approx \breve{u}_i^m(\boldsymbol{x}_p^m) \ , \quad p = 1, N_u \tag{10}$$

where superscript m indicates a quantity associated with a measurement, which is approximate due to normal experimental errors (e.g. noise), and N_u is the number of positions in space where measurements are taken. It should be noted that equation (9) cannot be used directly because, in soft tissue, due to the nearly incompressible behavior, $\breve{u}_{k,k}$ is a very small number multiplied by the very large number λ. Thus, small errors in the data lead to very large errors in p. So the hydrostatic stress, $\breve{p}(\boldsymbol{x})$, must also be solved for, where it is whatever it needs to be to best satisfy the balance of linear momentum (8).

2.3 Finite Element Approximation

In this paper, the finite element method is used to approximate the governing equations. The displacement field, $\breve{\boldsymbol{u}}(\boldsymbol{x}, t)$, hydrostatic stress, $\breve{p}(\boldsymbol{x}, t)$, and shear modulus $\mu(\boldsymbol{x})$ in (8) are approximated as

$$\breve{u}_i(\boldsymbol{x}) \approx \breve{u}_i^h(\boldsymbol{x}) = \bar{u}_{i\alpha}\psi_\alpha(\boldsymbol{x}) \tag{11}$$

$$\breve{p}(\boldsymbol{x}) \approx \breve{p}^h(\boldsymbol{x}) = \bar{p}_\gamma\tilde{\breve{\psi}}_\gamma(\boldsymbol{x}) \tag{12}$$

$$\mu(\boldsymbol{x}) \approx \mu^h(\boldsymbol{x}) = \bar{\mu}_\eta\breve{\psi}_\eta(\boldsymbol{x}) \tag{13}$$

where superscript h represents the approximate functions in the finite dimensional space and $\psi_\alpha(\boldsymbol{x})$, $\tilde{\breve{\psi}}_\gamma(\boldsymbol{x})$, and $\breve{\psi}_\eta(\boldsymbol{x})$ are the finite element shape functions for the displacement, hydrostatic stress, and shear modulus fields, respectively. Greek subscripts refer to node (or shape function) number, and Roman subscripts refer to spatial degrees of freedom. Taking the weak form of equation (8) and substituting in the finite dimensional approximations, yields

$$\int_\Omega \left\{ \left[\mu^h \left(\breve{u}_{i,j}^h + \breve{u}_{j,i}^h\right) + \breve{p}^h\delta_{ij}\right] w_{i,j}^h - \rho\omega^2\breve{u}_i^h w_i^h \right\} \, dV = \int_{\partial\Omega_2} \hat{T}_i w_i^h \, dA \tag{14}$$

for arbitrary trial functions, $w_i^h(\boldsymbol{x}) = \bar{w}_{i\beta}\psi_\beta(\boldsymbol{x})$ and $q^h(\boldsymbol{x}) = \bar{q}_\rho\tilde{\breve{\psi}}_\rho(\boldsymbol{x})$. Likewise, equation (9) takes on the form

$$\int_\Omega \left(\breve{u}_{i,i}^h - \frac{\breve{p}^h}{\lambda}\right) q^h \, dV = 0 \tag{15}$$

In the usual forward problem, the shear modulus field, μ^h, is specified together with boundary conditions on the displacements and/or tractions (3) and (4), and equations (14) and (15) can be solved for the displacement and hydrostatic stress fields, $\breve{\boldsymbol{u}}^h$ and $\breve{p}^h$, on the domain, which is reduced to solving for the coefficients of the interpolants, $\bar{u}_{i\alpha}$ and $\bar{p}_\gamma$. However, it is important to note that an appropriate choice of finite element interpolants for the displacement ($\psi_\alpha(\boldsymbol{x})$) and hydrostatic stress ($\tilde{\breve{\psi}}_\gamma(\boldsymbol{x})$) fields is needed for stability, satisfying the so-called Babuška-Brezzi condition [3], due to the nearly incompressible behavior. For time harmonic cases, the solution is naturally oscillatory, and sufficiently fine meshes, for the given interpolation order, are needed to accurately capture the solution and assure h-convergence (i.e. convergence on the solution with respect to the mesh size).

In the inverse problem, which will be described in more detail in the next section, displacements are known approximately at discrete locations. If we define our finite element mesh so that our nodes align with these discrete locations, then we know approximately, $\bar{u}_{i\alpha}$ (assuming standard interpolation functions), and the goal is to determine the shear modulus field $\bar{\mu}_\eta$. It is important to note that, instead of boundary conditions, the displacement field is known throughout the domain approximately. Furthermore, due to the measurement techniques, the measurements at the boundaries of the domain likely have the least accuracy.

3. INVERSE PROBLEM SOLUTION APPROACH

In solving the inverse problem described in the previous section, several important issues arise. First, the displacement data is only known approximately, and derivatives of the displacement data appear in our governing equations. Directly differentiating noisy data will cause very big errors in the solution. Second, the displacement data is only known at discrete locations, which may not be sufficiently, finely spaced to satisfy mesh convergence in the forward solution. Third, as mentioned above, the measured displacements are throughout the domain, not just at the boundary, and, in fact, the measured displacements at the boundary are probably least accurate, so should not be over-weighted in the solution.

Two solution approaches will be described next along with discussions regarding the strength and weakness of each with regard to the issues mentioned in the previous paragraph. The first approach, we refer to as a direct approach, uses smoothed displacement data directly in equation (14) and solves for nodal values of the shear modulus, $\bar{\mu}_\eta$, and hydrostatic stress, $\bar{p}_\gamma$. The second approach, we refer to as an iterative approach, solves the optimization problem that finds the nodal values of the shear modulus that gives nodal displacements, $\bar{u}_{i\alpha}$, from a direct solution that are close to the measured values and satisfy the governing equations (14) and (15). The iterative approach described here is very similar to the approach used by van Houten *et al.* [7].

3.1 Direct Approach

In the direct approach, the problem solved on the finite dimensional space is find $\mu^h(\boldsymbol{x})$ and $\check{p}^h(\boldsymbol{x})$ that best satisfy equation (14), where the displacement field, $\boldsymbol{u}^h(\boldsymbol{x})$, is specified to be a smoothed, volume-preserving field close to the measured displacement field. In this work, a Gaussian filter is used to smooth the displacement data.

One problem remains, and that is dealing with the term on the right-hand-side of (14), which is associated with the traction boundary condition (4). There are two possible approachs. The simplest approach is to impose displacement boundary conditions on the entire boundary using the smoothed values close to the measured values. However, this treats those displacements as exact, over-weighting the boundary displacements, which are probably the least accurate. An alternative is to make no assumption about the boundary conditions, but rather, assemble the system of equations not including the equations associated with the unknown boundary conditions. This can be thought of as moving the boundary in by one layer of elements, and using the outer layer equations to apply the boundary conditions on the reduced domain. However, this reduces the number of equations available and can lead to an indeterminate system, since the equations associated with that outer layer of elements are in terms of the sought shear modulus, $\mu^h(\boldsymbol{x})$, and hydrostatic stress, $\check{p}^h(\boldsymbol{x})$, in those elements. In this work, the values of $\mu^h(\boldsymbol{x})$ and $\check{p}^h(\boldsymbol{x})$ in the outer layer of elements are assumed to be extrapolated values from the nearest neighboring element on the interior, in order to reduce the number of unknowns.

The advantages of the direct approach described above are that it does not require iterations and can be performed on any subdomain of the observed region, and is thus, fast. In addition, it does not over-weigh boundary data, but rather treats all the data equally. On the down side, the data needs to be filtered and differentiated.

3.2 Iterative Approach

In the iterative approach, the problem to be solved is to find $\mu^h(\boldsymbol{x})$ and $\check{p}^h(\boldsymbol{x})$ that minimize

$$\min_{\mu^h, \check{p}^h} \left[\frac{1}{2} \sum_{\alpha=1}^{N_p} \left(\check{u}_i^h(\boldsymbol{x}_\alpha) - \check{u}_i^m(\boldsymbol{x}_\alpha) \right) \right] \tag{16}$$

where $\check{u}_i^h(\boldsymbol{x})$ is the displacement field satisfying equations (14) and (15) depending on $\mu^h(\boldsymbol{x})$ and $\check{p}^h(\boldsymbol{x})$. Although the governing equations are linear, the minimization results in a non-linear system, which must be solved iteratively. A similar approach was used by van Houten *et al.* [7], but, in that work, the authors solved for μ^h and λ^h (instead of $\check{p}^h$). Since the material is relatively incompressible and since the parameter λ varies on the order of only 5% in soft tissue, it seems more reasonable and stable to fix λ, which is roughly the bulk modulus of water, and solve for the hydrostatic stress field.

The advantage of this approach is that it does not require differentiation of the data and uses the data directly, not requiring any filtering. The disadvantages are that the procedure is slow because it is iterative and requires a full forward solution on each iteration.

4. NUMERICAL EXPERIMENTS

A simple 2-dimensional example involving simulated data of a square domain with a square inclusion is used to demonstrate the direct algorithm and also investigate the effect of neglecting the hydrostatic stress term in equation (8). The problem geometry is shown in Figure 1. Plane strain conditions are assumed. The size of the overall domain is 50 mm on a side. At the center, there is a stiff square inclusion that is 15 mm x 15 mm. The background is assumed to have a shear modulus of 9 kPa while the inclusion has a stiffness of 18 kPa. These are typical stiffnesses for soft tissue. The density is set to 1000kg/m^3. We apply a 50Hz sinusoidal excitation which has 1mm amplitude in the horizontal direction on the bottom surface. All other boundaries are traction free.

Synthetic displacement data are generated with a forward finite element solution. To imitate the experiment, we collect the steady state time harmonic displacement data within the square 40mm x

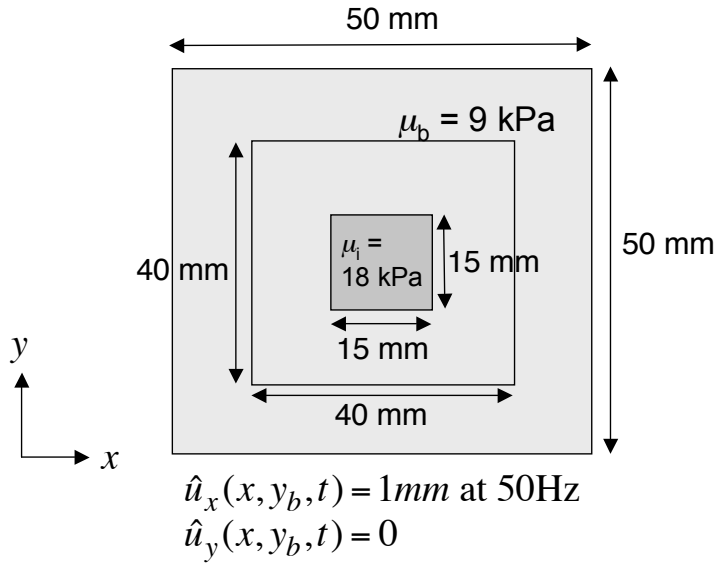

Figure 1: Square shaped single inclusion case. Total size is 50mm x 50 mm which has a 15mm x 15 mm square inclusion. Displacement data are "collected" in the interior 40mm x 40mm region.

40mm interior region. Bi-linear quadratic interpolants are used for the displacement field and piecewise constant interpolants are used for the hydrostatic stress field (Q1/P0 elements). The element size which is used for the forward data fabrication is 0.25mm × 0.25mm resulting in a mesh with 40,000 elements. A sequence of meshes was used to verify the convergence in the forward problem solution.

For the inverse problem, a much coarser mesh is used with an element size of 1mm × 1mm, which is sixteen times large than the element size used in the forward solution and is comparable to experimental resolution. Two reasons for using a coarser mesh for the inverse solution are as follows: (a) primarily because experimental data is typically taken on a grid with grid points on the order of one mm apart, and we want to test our algorithm on simulated data that is similar to actual physical data, which our algorithm will need to handle to be satisfactory, and (b) to properly test the algorithm, it is important that the model used for the inverse problem be different from that used in the forward model to generate the data. The displacement data from the forward solution is down-sampled at the nodes of the coarse mesh, which contains 1681 grid points (nodes). Q1/P0 elements are used for the displacement/hydrostatic stress fields, and P0 (piecewise constant) elements are used for the shear modulus field. The direct approach described in Section 3.1 is used to solve the inverse problem using the down-sampled simulated data as well as noisy data. To fabricate the noisy data, denoted $\tilde{\boldsymbol{u}}(\boldsymbol{x})$, we added Gaussian random noise as follows

$$\tilde{\boldsymbol{u}}(\boldsymbol{x}) = \check{\boldsymbol{u}}(\boldsymbol{x}) + \check{\boldsymbol{u}}_{avg}\varepsilon(\boldsymbol{x}) \tag{17}$$

where $\varepsilon(\boldsymbol{x})$ has a Gaussian random distribution whose mean is zero and standard deviation is 3%, and $\check{\boldsymbol{u}}_{avg}$ is the mean average of the displacement components in the region of interest.

Results for the shear modulus recovery are shown in Figure 2. Figure 2(a) shows the specified shear modulus field, and Figure 2(b) shows the recovered shear modulus field using the computed displacements in the region of interest at the nodes on the coarse mesh used in the inversion. On the back side of the inclusion, the solution is not good because of the small displacements in this region providing little information. The information content becomes less as the distance from the excitation becomes greater (signal to "noise" is going down). It should also be noted that the mesh used for the inverse problem is not fine enough to give an accurate solution to the forward problem, so it is not surprising that the inverse solution has some inaccuracy. Again, the reason for the coarse mesh is because real data is typically on a grid similar to that used here, and one of the goals is to test the algorithm on data similar to experimental data. To see the effect of noise in the data, the result using the unfiltered noisy data, as specified in the previous paragraph, are shown in Figure 2(c). After applying a Gaussian filter with a width of 15 elements and a standard deviation of 2%, the result shown in Figure 2(d) is obtained. The result in both Figures 2(b) and 2(d) tends to underestimate the stiffness on the side of the inclusion closest to the excitation, and slightly overestimate the stiffness on the back side. The boundaries of the inclusion

are also blurred due to the smoothing of the data, coarse mesh, and natural instability in the solution approach (i.e. different shear modulus fields give similar displacement fields).

To see the effect of the hydrostatic stress, first, we look at the hydrostatic stress field, and we look at the solution obtained neglecting the hydrostatic stress gradient in the equations of elasto-dynamics (i.e. neglect the term $p_{,i}$ or $\check{p}_{,i}$ in equations (1) and (8)). The reason we look at this is because, as mentioned in the introduction, most researchers neglect this term in order to simplify the equations. First, the hydrostatic stress recovered in the forward solution, on the fine mesh, is shown in Figure 3(a), and that recovered in the inverse solution procedure, on the coarse mesh with the computed displacements from the forward solution used as input, is shown in Figure 3(b). The pressure recovery is pretty good, although a little smoothed out. From this result, it appears that there are some non-negligible gradients in the hydrostatic stress field. Finally, Figure 4 shows the shear modulus recovery using the direct approach including the hydrostatic term (b) and neglecting it (c). Figure 4(a) shows the target solution on the same scale. While the inclusion is still easily seen in the case neglecting the hydrostatic stress, the recovered values for the shear modulus are much lower than they should be, and even negative in some regions. On this scale, the solution including the hydrostatic term looks very good, except on the far side of the inclusion.

Although this example problem is simplistic and the results presented are qualitative, the results illustrate a few key points. These are: (i) the direct approach presented is a viable approach, (ii) for an accurate reconstruction, the gradient of the pressure field should not be neglected (even in this simple example, it has a strong effect), and (iii) the grid that experimental data is taken on may be coarser than that required for an accurate interpolation. With regard to point (i), this algorithm has recently been applied to MRI data taken on a tissue-mimicking phantom with very good results, which are in the process of being documented. With regard to point (iii), the issue of resolution on a typical experimental grid needs further quantitative analysis and needs to be compared against competing algorithms.

5. CONCLUSIONS AND FUTURE WORK

Two methods for reconstructing the shear modulus field in soft tissue given measured interior displacements for time harmonic excitations are discussed. The direct method requires differentiating the data, and thus requires some preprocessing of the data to remove noise, but does not require iterations and equally weights all the data. The iterative method does not require differentiating the data, but does require iterations with a full forward solution on each iteration. In order to obtain the forward solution, boundary conditions are required. Typically, the displacement data is used for this, which over-weights the data on the boundary. Results from the direct method are shown for a simple two-dimensional, plane strain case, with a single, square inclusion. Simulated data from a forward finite element solution on a very fine mesh is used. The effect of adding noise and then using a noise removal algorithm before the direct inversion algorithm was investigated. Good results were obtained with the inclusion being detected and the value of the shear modulus close to the correct value. However, the boundary of the inclusion is smeared, due to the smoothing of the noisy data, the coarse mesh resolution in the inverse problem, and the natural instability of the solution. Also, further from the excitation, where the signal to noise ratio is less, the solution is deteriorated, especially on the far side of the inclusion. Future work will test the direct inversion method with more complicated geometries and inclusions, in both 2- and 3-dimensions. More quantitative studies investigating error and resolution and comparing against other algorithms are on-going. We are also beginning to test the algorithm with phantom data. In addition, we are developing an approach to extend the direct inversion approach to the transient case. It is expected that with time dependent data, an improved solution can be obtained because of the richer data set [13]. Finally, we are starting to investigate anisotropic and viscoelastic effects.

Acknowledgement

This work has been supported by the National Science Foundation through grant DMS-0101458 and by the National Institutes of Health through grant 5 R21 EB003000-02. The authors thank J. McLaughlin, J-R. Yoon, and D. Renzi in the Mathematical Sciences Department at Rensselaer for many valuable discussions.

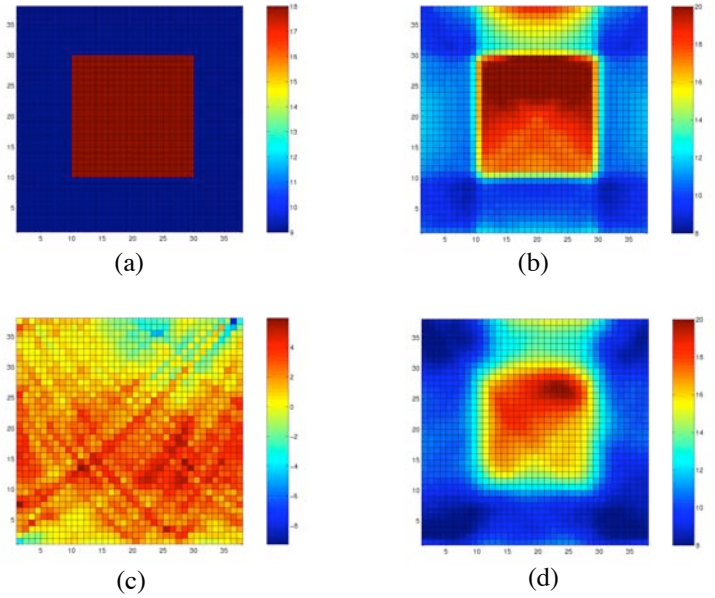

Figure 2: Results for shear modulus recovery (a) specified values (exact solution), (b) recovery using exact finite element forward solution data (down-sampled to inverse problem mesh), (c) recovery using noisy data without filtering, and (d) recovery using filtered data. Scale for (a) is 9-18 kPa, (b) 9-20 kPa, (c) -9 to 6 kPa, and (d) 8-20 kPa. Only the central portion of the domain considered is shown.

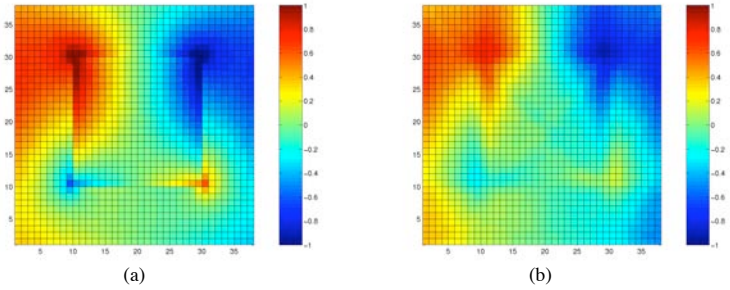

Figure 3: Hydrostatic stress distribution in region of interest (a) from forward solution and (b) recovered in inverse problem solution. Scale from -1 to 1 kPa.

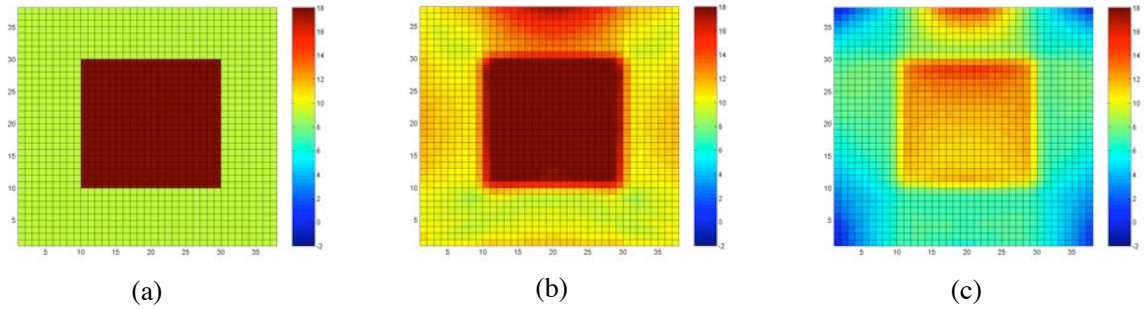

Figure 4: Shear modulus recovery investigating effect of hydrostatic stress field: (a) specified values (exact solution), (b) recovery using exact finite element forward solution data including hydrostatic stress term, and (c) recovery neglecting hydrostatic stress term. The scale, in each case, is from -2 to 18 kPa.

REFERENCES

1. P. Barbone and J. Bamber, Quantitative elasticity imaging: What can and cannot be inferred from strain images. *Phys. Med. Biol.* (2002), Vol. **47**, 2147–2164.

2. J. Bercoff, S. Chaffai, M. Tanter, L. Sandrin, S. Catheline, M. Fink, J. L. Gennisson and M. Meunier, In vivo breast tumor detection using transient elastography. *Ultrasound in Med. & Biol.* (2003), Vol. **29**, 1387–1396.

3. F. Brezzi and M. Fortin, *Mixed and hybrid finite element methods,* Springer, New York, 1991.

4. S. Catheline, J. L.Thomas, F. Wu and M. Fink, Diffraction field of a low frequency vibrator in soft tissues using transient elastography. *IEEE Trans. Ultrason. Ferroelect. and Freq. Cont.* (1999), Vol. **46**, 1013–1019.

5. Y.C. Fung, *Biomechanics: Mechanical Properties of Living Tissue*, New York, Springer-Verlag, 1993.

6. E. van Houten, K. Paulsen, M. Miga, F. Kennedy and J. Weaver, An overlapping subzone technique for MR-based elastic property reconstruction. *Magn. Reson. Med.* (1999), Vol. **42**, 779–786.

7. E. van Houten, M. Miga, J. Weaver, F. Kennedy and K. Paulsen, Three-dimensional subzone-based reconstruction algorithm for MR elastography. *Magn. Reson. Med.* (2001), Vol. **45**, 827–837.

8. S.-R. Huang, R. Lerner and K. Parker, Time domain doppler estimators of the amplitude of vibrating targets. *J. Acoust. Soc. Am.* (1992), Vol. **91**, 965–974.

9. E. Konofagou and K. Hynynen, Localized harmonic motion imaging: Theory, simulations and experiments. *Ultrasound in Med. & Biol.* (2003), Vol. **29**, 1405–1413.

10. E. Konofagou and J. Ophir, A new elastographic method for estimation and imaging of lateral displacements, lateral strains, corrected axial strains and poisson's ratios in tissues. *Ultrasound in Med. & Biol.* (1998), Vol. **24**, 1183–1199.

11. T. Krouskop, T. Wheeler, F. Kallel, B. Garra and T. Hall, Elastic moduli of breast and prostrate tissues under compression. *Ultrasonic Imaging* (1998), Vol. **20**, 260–274.

12. A. Manduca, D. Lake, S. Kruse and R. Ehman, Spatio-temporal directional filtering for improved inversion of MR elastography images. *Medical Imaging Analysis* (2003), Vol. **7**, 465–473.

13. J.R. McLaughlin and J-R. Yoon, Unique identifiability of elastic parameters from time-dependent interior displacement measurement. *Inverse Problems* (2004), Vol. **20**, 25–45.

14. J. Ophir, I. Céspedes, H. Ponnekanti, Y. Yazdi and X. Li, Elastography: A quantitative method for imaging the elasticity of biological tissues. *Ultrasonic Imaging* (1991), Vol. **13**, 111–134.

15. J. Ophir, F. Kallel, T. Varghese, E. Konofagou, S. Alam, T. Krouskop, B. Garra and R. Righetti, Elastography, optical and acoustic imaging of acoustic media. *CR Acad. Sci. Paris* (2001), Vol. **2**, 1193–1212.

16. A. Sarvanzyan, Shear acoustic properties of soft biological tissues in medical diagnostics. *J. Acoustic Soc. Am.* (1993), Vol. **93**, 2329–2330.

17. R. Sinkus, J. Lorenzen, D. Schrader, M. Lorenzen, M. Dargatz and D. Holz, High-resolution tensor MR elastography for breast tumour detection. *Phys. Med. Biol.* (2000), Vol. **45**, 1649–1664.

18. M. Tanter, J. Bercoff, L. Sandrin and M. Fink, Ultrafast compound imaging for 2-d motion vector estimation: Application to transient elastography. *IEEE Trans. Ultrason. Ferroelect. and Freq. Cont.* (2002), Vol. **49**, 1363–1374.

19. M. Walz, J. Teubner and M. Georgi, Elasticity of benign and malignant breast lesions, imaging, applications and results in clinical and general practice, *Eighth International Congress on the Ultrasonic Examination of the Breast*, 1993, p. 56.

20. Z. Wu, L. S. Taylor, D. J. Rubens and K. J. Parker, Shear wave focusing and three-dimensional sonoelastography. *J. Acoust. Soc. Am.* (2002), Vol. **111**, 439–446.